

# **Feasibility of Free Radical Polymerization of Acrylic Acid in a Continuous Flow Reactor**

by

**Joshua David Ward**

Bachelor of Science in Chemistry, Clarion University of Pennsylvania, 2014

Submitted to the Graduate Faculty of the  
Swanson School of Engineering in partial fulfillment  
of the requirements for the degree of  
Master of Science in Materials Science and Engineering

University of Pittsburgh

2021

UNIVERSITY OF PITTSBURGH

SWANSON SCHOOL OF ENGINEERING

This thesis was presented

by

**Joshua David Ward**

It was defended on

March 19, 2021

and approved by

Lei Li, PhD, Associate Professor, Department of Chemical and Petroleum Engineering

Xiayun Zhao, PhD, Assistant Professor, Department of Mechanical Engineering and Materials  
Science

Thesis Advisor: Sachin Velankar, PhD, Professor, Department of Chemical and Petroleum  
Engineering & Department of Mechanical Engineering and Materials Science

Copyright © by Joshua David Ward

2021

# Feasibility of Free Radical Polymerization of Acrylic Acid in a Continuous Flow Reactor

Joshua David Ward, MS

University of Pittsburgh, 2021

The polymerization kinetics and feasibility of producing polyacrylic acid in water with ammonium persulfate via a lab-scale continuous flow tubular reactor was investigated. Initial monomer concentrations ranging from 0.70 to 3.00 mol/L and initiator concentrations ranging from 0.056 to 0.112 mol/L were tested at 90 °C. The reactor included two HPLC pumps, two static mixers, and disposable PTFE tubing in a hot bath. A product closely meeting the industrially-desired values of molecular weight 300,000 g/mol, polydispersity index of 10, 25% solids, and acrylic acid conversion  $\geq 99.0\%$  was successfully manufactured. However, high monomer concentrations lead to significant fouling challenges which pose a serious concern for industrial application. The pseudo steady-state kinetics of acrylic acid polymerization was studied and the effects of initial monomer and initiator concentrations and residence times were investigated. Experimental results agree with past reports that conversion increases with initial monomer concentration and that the polymerization rate has a  $3/2$  power dependence on monomer concentration as opposed to the conventional 1st power dependence found within other free radical polymerizations. A simple simulation of the polymerization of acrylic acid was created based on the reviewed kinetics. This simulation is still in its early stages and does not yet accurately model every kinetic consideration. A more robust simulation would provide support to future experiments by accurately predicting final polymer properties based on initial conditions.

## Table of Contents

Preface.....	xi
1.0 Introduction.....	1
2.0 Background .....	2
2.1 Batch Vs Continuous .....	2
2.2 Free Radical Polymerization and Kinetics of Acrylic Acid Polymerization .....	4
2.3 Rate Constants .....	10
3.0 Experimental Setup .....	13
3.1 FlowSyn System and Additional Components.....	13
3.2 Chemicals .....	15
3.3 General Lab Procedure.....	15
3.4 Sample Characterizations.....	19
4.0 Results and Discussion.....	21
4.1 Effect of Different Parameters .....	25
4.1.1 Initial Monomer Concentration.....	25
4.1.2 Initial Initiator.....	26
4.1.3 Residence Time.....	26
4.1.4 Temperature .....	27
4.1.5 Polydispersity Index.....	27
4.2 Tube Fouling .....	28
4.3 Simulation .....	31
5.0 Conclusion .....	36

<b>6.0 Future Work.....</b>	<b>37</b>
<b>Appendix A .....</b>	<b>38</b>
<b>Bibliography .....</b>	<b>41</b>

## List of Tables

<b>Table 1: Borisov's APS rate constants as a function of initial concentration and temperature<sup>13</sup> .....</b>	<b>10</b>
<b>Table 2: Estimated rate constants at varying initial concentrations and 90 °C.....</b>	<b>12</b>
<b>Table 3: General trends when increasing residence time, and initial monomer and initiator concentrations. ....</b>	<b>23</b>
<b>Table 4: PAA products at same initial concentrations but at different temperatures .....</b>	<b>27</b>
<b>Appendix Table 1: All data used for Figures 7-9.....</b>	<b>40</b>

## List of Figures

<b>Figure 1: AA monomer conversion at 65% neutralization and 55°C with time at varying initial monomer concentrations; from Cutie et al.<sup>14</sup>.....</b>	<b>6</b>
<b>Figure 2: Effect of monomer concentration on AA polymerization rate. (a) Cutie et al.<sup>14</sup> (b) Qiu et al.<sup>6</sup>.....</b>	<b>7</b>
<b>Figure 3: FlowSyn setup for the continuous flow production of polyacrylic acid .....</b>	<b>13</b>
<b>Figure 4: PAA boiling immediately after sample collection .....</b>	<b>17</b>
<b>Figure 5: Clean PTFE tube (top) compared to tube with polymer fouling (bottom). .....</b>	<b>19</b>
<b>Figure 6: GPC data for sample of <math>[M]_0 = 2.92</math>, <math>[I]_0 = 0.077</math> and 2 minute residence time provided by Lubrizol .....</b>	<b>20</b>
<b>Figure 7: PAA product molecular weight with residence time at various initial concentrations. ....</b>	<b>22</b>
<b>Figure 8: PAA product polydispersity with residence time at various initial concentrations. ....</b>	<b>22</b>
<b>Figure 9: PAA product % monomer conversion with residence time at various initial concentrations. ....</b>	<b>23</b>
<b>Figure 10: MW and % conversion over 8 hour period of sample collection.....</b>	<b>24</b>
<b>Figure 11: Vernier pressure reading of high monomer concentration (3.0 M) polymerization run.....</b>	<b>29</b>
<b>Figure 12: String of previously stuck polymer extruding out.....</b>	<b>30</b>
<b>Figure 13: MATLAB simulation for polymerization of AA with APS at low and high <math>[M]_0</math> .....</b>	<b>32</b>

**Figure 14: Zoomed in view of  $[I]$ ,  $[2Rc \cdot]$ ,  $[R \cdot]$ , and  $[RM \cdot]$ , at  $90^\circ\text{C}$ ,  $[M]_0 = 0.7$  and  $[I]_0 = 0.056 \text{ mol/L}$  at very short RT ..... 34**

**Appendix Figure 1: Additional calculation steps for final polymerization rate ..... 38**

**Appendix Figure 2: 18 simulation graphs depicting monomer consumption rate at different parameters over 10 min RT. .... 39**

## List of Schemes

<b>Scheme 1: FRP steps for AA with APS.....</b>	<b>5</b>
<b>Scheme 2: Proposed mechanism and corresponding reaction rates of FRP of AA. Together, steps 1, 2 and 3 are the initiation<sup>14</sup>.....</b>	<b>8</b>
<b>Scheme 3: Mechanism for 1,5- hydrogen shift backbitting by Wittenberg<sup>16</sup>.....</b>	<b>11</b>

## Preface

I sincerely want to thank my research advisors, Dr. Sachin Velankar and Dr. Lei Li, for their trust in me to bring value to this research. From Sachin's probing questions to Lei's encouragement, their guidance and support during my time at the University of Pittsburgh has been invaluable. In my lab work, Sugandhika Samdhian and Robin Thomas gave much assistance to me.

I would like to acknowledge the members of Lubrizol; John Dietrich, Glenn Cormack, and Cliff Kowall, for their input and guidance. Additionally, I appreciate the characterization work of Lubrizol's analytical team. This research would not have been possible without the financial support and strong partnership that Lubrizol has with the University of Pittsburgh.

I praise God for his blessings upon me during my time at the University of Pittsburgh.

*Soli Deo Gloria*

## 1.0 Introduction

This paper's research has benefitted from industrial-academia collaboration. Lubrizol is a provider of specialty chemicals and has had a good working relationship with the University of Pittsburgh for many years. They are considering converting some of their processes from batch to continuous flow (CF). Lubrizol's Polyacrylic acid (PAA) is used in formulations for personal care products such as shampoo, thus they require near 100% conversion of the acrylic acid (AA) monomer.

The main objective of this research was to investigate the kinetics and feasibility of producing polyacrylic acid (PAA) via free radical polymerization in a CF tubular reactor at high starting concentrations. Being a linear polymer that only requires one monomer, one initiator, and water as a solvent, PAA is a good candidate to transition from batch to continuous manufacturing. If deemed feasible, there are many benefits to producing fast reacting and highly exothermic polymers via tubular CF rather than a batch reactor, such as: a reduction in equipment size, more consistent heat transfer, reduction in energy consumptions, reduced manpower, and a reduction of waste.

## 2.0 Background

### 2.1 Batch Vs Continuous

Traditionally, numerous reactions in the chemical industry have taken place using batch reactors rather than tubular CF reactors. Even though the advantages to converting over to tubular CF are numerous (as a form of process intensification), continuous processing technologies have been slow to make their way into industrial chemical synthesis, possibly due to a reliance on traditional methods and high revenues with a lack of competition<sup>1</sup>. However, increased globalization and shrinking major markets will likely drive industries away from technological stagnation<sup>1</sup>.

Especially when considering highly exothermic reactions, batch reactors are prone to temperature fluctuations (due to poor heat dissipation and hotspots)<sup>2</sup> and are difficult to scale up for this reason<sup>3,4</sup>. In the last two decades, research on replacing batch reactors with continuous flow reactors has become more prominent for organic chemistry synthesis<sup>4-6</sup>; this even includes macromolecules such as polymers<sup>2,3</sup>.

Primarily due to their large surface to volume ratios, tubular CF reactors have excellent mass and heat transfer properties<sup>2-5,7,8</sup>. An immediate consequence of this is a better level of control and response times. Compared to batch reactors, CF has quicker processing times<sup>3,4,7</sup>, lower production costs<sup>3</sup>, and a smaller equipment footprint that leads to a safer<sup>2-4,6,7</sup> and more environmentally friendly process<sup>3,7</sup>. Additionally, scaling-up CF reactors is relatively simple as the flow rate and reactor length (volume) can easily be modified to suit larger production scales<sup>2,4,7</sup>. Two other benefits of tubular CF reactors are the ability to continuously produce

product without stopping and to increase production by running multiple smaller-scale tubular CF reactors in parallel (numbering up)<sup>2</sup>. An additional advantage of numbering up is that maintenance on one unit will not impede the production of the other units. When specifically considering highly exothermic reactions, tubular CF provides an opportunity for the process to be isothermal.<sup>2-4,6,8</sup> All these advantages are why many consider tubular CF better for chemical synthesis, especially for fast and highly exothermic reactions<sup>2-4,6,8</sup>.

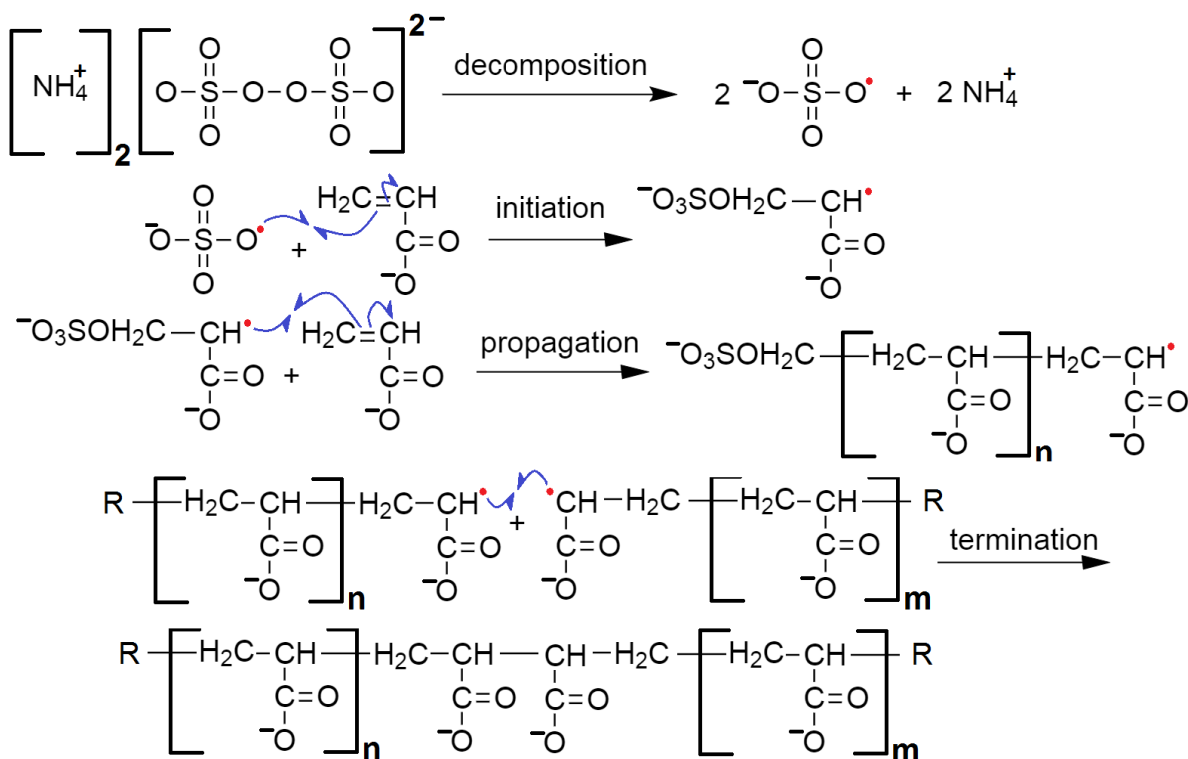
A disadvantage of tubular CF operations is the potential for the tubing to accumulate fouling<sup>9</sup>. Fouling occurs when processed material sticks to the side of the reactor tubing and causes disruptions. Among these problems are reduced heat transfer and potential blockages. Heat transfer is reduced due the foulant acting as an insulating barrier that diminishes external heating effects. Partial or even full blockages can occur in the tubing when enough foulant builds up. Even when a full blockage doesn't occur, chunks of foulant may dislodge and be collected as product. Batch processes do experience fouling as well, but they are often cleaned in between batches and more easily than tubular reactors.

Due to better reactant mixing, heat transfer, and more controlled reaction times, tubular CF reactors also provide a better way to investigate reaction kinetics under isothermal conditions<sup>5,6</sup>. Brocken et al. and Qiu et al. have investigated the continuous production of PAA<sup>5,6</sup>. Brocken's research used a FlowSyn instrument to screen and determine the processing conditions of PAA production at very low initial monomer and initiator concentrations (0.4-1.0 mM and 0.005-0.0375 mM respectively)<sup>5</sup>. Qiu's research employed a custom tubular CF system that avoided the need to change the flow rate to alter the residence time<sup>6</sup>. Qiu's research tested initial monomer and initiator concentrations ranging from 0.35-1.40 M and 0.056-0.112 M,

respectively, and focused on the kinetics of PAA polymerization. Neither paper reported any fouling.

## **2.2 Free Radical Polymerization and Kinetics of Acrylic Acid Polymerization**

Free radical polymerization (FRP) is a specific type of addition polymerization that can produce long chains from monomers with the general structure of  $H_2C=CR_1R_2$ . The reactivity of the carbon-to-carbon pi bonds lends itself to easy attack from free radical or ionic initiators<sup>10</sup>. The conversion of these pi bonds into sigma bonds is the primary reason why free radical polymerizations are exothermic, even to the point of explosion if the reaction runs away<sup>11</sup>. It is well known that FRPs have three primary stages: initiation, propagation, and termination<sup>10</sup>. Scheme 1 shows these steps for FRP of acrylic acid (AA) with ammonium persulfate (APS), (the initiation step involves decomposition plus initiation).



**Scheme 1: FRP steps for AA with APS.**

The initiator for FRP is usually a peroxide or azo compound<sup>11,12</sup>. For the AA polymerization in this research, APS is used. During decomposition, APS thermally decomposes to form two free radicals with an activation energy ( $E_a$ ) of approximately 52 kJ/mol<sup>13</sup>. During initiation, the free radical attacks the carbon-to-carbon pi bonds on the monomer, changing them into a single sigma bond and then transfers over to one of the carbons. From here, propagation takes place whereby the same free radical attack occurs  $n$  times to connect  $n$  groups of monomers. The free radical is not consumed during this step and if it never is, then propagation could continue until all monomers have been consumed<sup>10</sup>.

Termination is the process by which a free radical is consumed and it can occur in two different ways, combination and disproportionation<sup>10,11</sup>. In combination (as shown in Scheme 1), two reactive radicals are removed by reacting with each other to form one stable and connected

product. In disproportionation, one free radical transfers an electron to another which results in two separate and stable products being formed.

Traditional FRP has a propagation rate proportional to the concentration of monomer times the  $1/2$  power of the initiator concentration ( $[M][I]^{1/2}$ )<sup>11</sup>. This propagation rate is based on the assumption of steady state kinetics whereby the concentration of free radicals will be constant at any point in time. With this propagation rate, conversion vs time is independent of monomer concentration<sup>10</sup>. However Cutie and Qiu et al. found that, in AA FRP, the rate of conversion with time is increased as the initial concentration of monomer is increased (Figures 1 and 2)<sup>6,14</sup>. From the least squares fitting, both Cutie and Qiu's data sets roughly agree with an ideal fit of 1.5 which shows a  $3/2$  dependence of monomer concentration on the polymerization rate. In both cases, the propagation rate has been determined to be  $[M]^{3/2}[I]^{1/2}$ <sup>6,14</sup>.

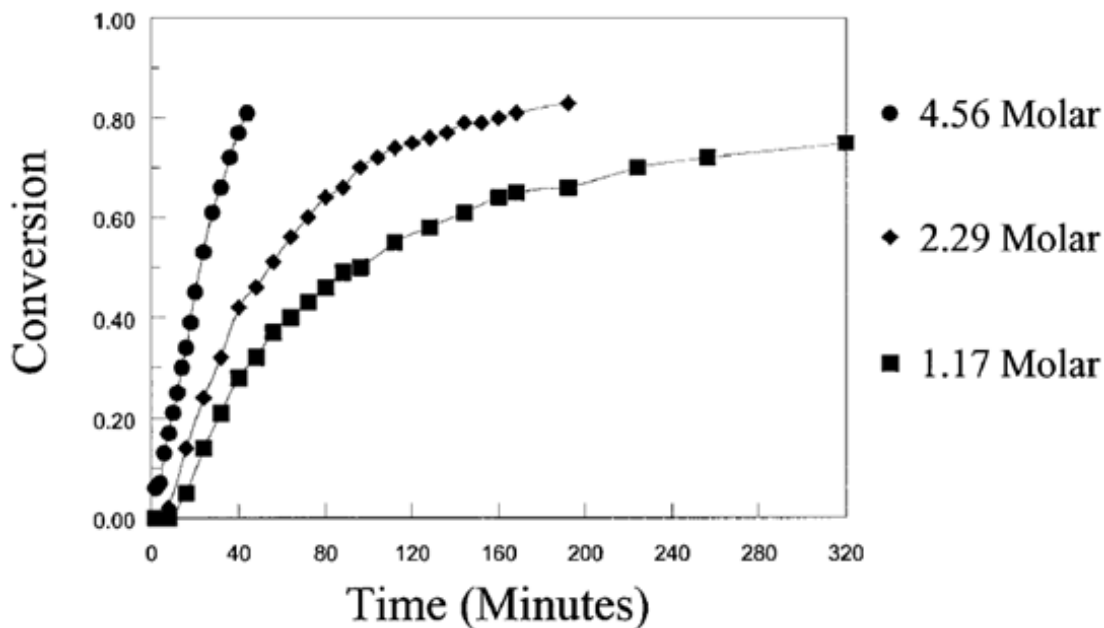


Figure 1: AA monomer conversion at 65% neutralization and 55°C with time at varying initial monomer concentrations; from Cutie et al.<sup>14</sup>.

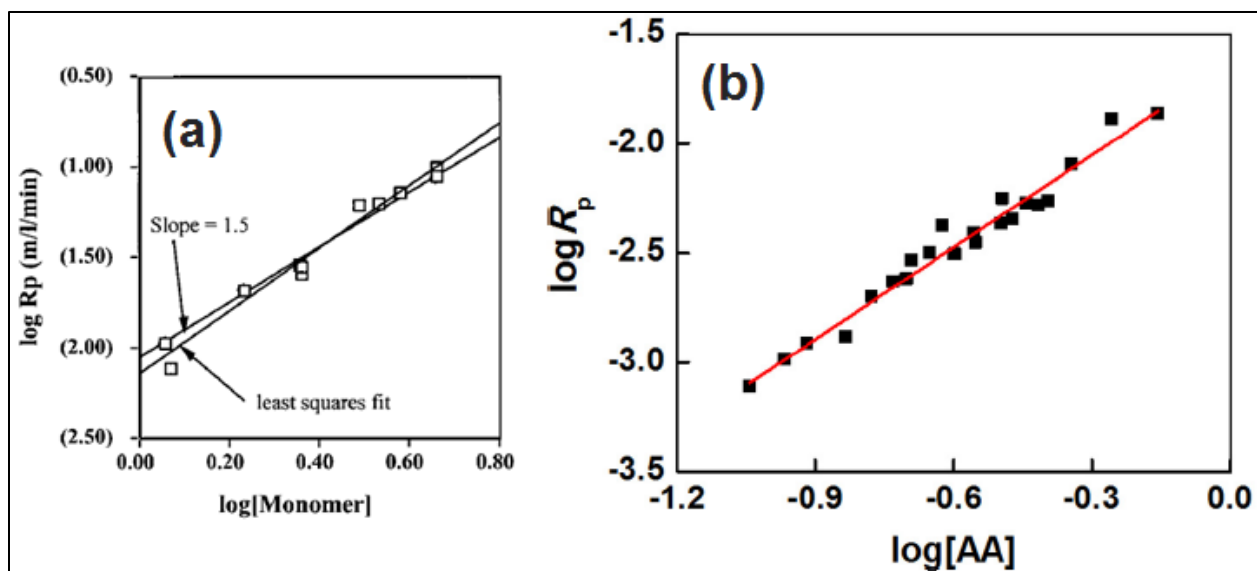
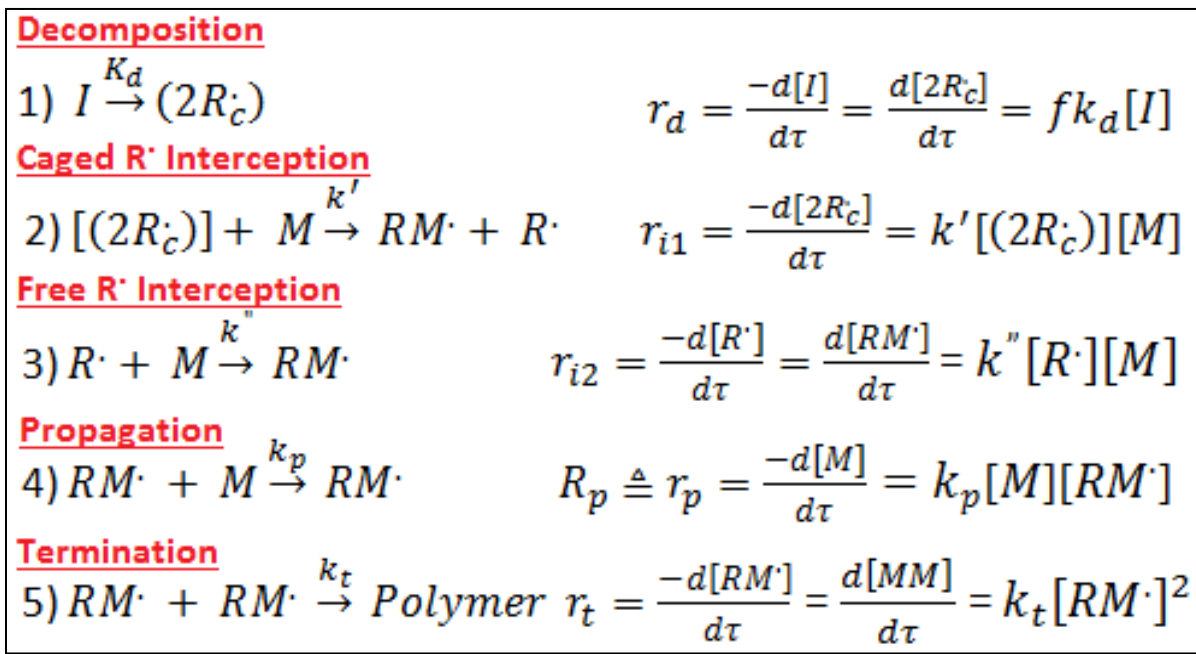


Figure 2: Effect of monomer concentration on AA polymerization rate. (a) Cutie et al.<sup>14</sup> (b) Qiu et al.<sup>6</sup>

To explain the difference of monomer concentration dependence on the propagation rates, APS in aqueous solution with AA has a much faster decomposition rate than that of typical FRP initiators (where their decomposition is the rate limiting step)<sup>10,12</sup>. In either case, most types of FRP initiators experience a "cage effect" whereby the newly produced free radicals are trapped within a cage of solvent molecules. When considering typical FRP initiators, the monomers react with their free radicals as soon as they decompose; (the existence of the cage effect doesn't change the propagation rate because the initiator decomposition is still the slowest step). However, for APS in aqueous solution, it quickly decomposes, but now, the caged free radicals may require a monomer to react with one of them which would then open up the cage to release the second free radical. This theory was proposed by Cutie et al. to explain the higher dependence on AA concentration for the propagation rate<sup>14</sup>.

Adapted from Cutie, Scheme 2 shows the kinetic scheme and corresponding reaction rates for the FRP of AA<sup>14</sup>. The interception of a caged free radical is shown as a separate step whose rate depends on the monomer concentration. Equations 2-1 - 2-5 show the rate

expressions for each species within FRP of AA and Equation 2-6 shows the final polymerization rate ( $R_p$ ) in terms of monomer and initiator concentrations. The various  $k$ 's are the rate constants for each process,  $f$  is an efficiency factor (taking into account that only some free radicals actually react with the monomers),  $R_c \cdot$  is a caged free radical while  $R \cdot$  is a free range radical, and  $R_p$  is the final polymerization rate for polyacrylic acid in terms of monomer and initiator concentration.



Scheme 2: Proposed mechanism and corresponding reaction rates of FRP of AA. Together, steps 1, 2 and 3 are the initiation<sup>14</sup>.

$$\frac{d[I]}{d\tau} = -fk_d[I] \quad (2-1)$$

$$\frac{d[2R_c\cdot]}{d\tau} = fk_d[I] - k'[(2R_c\cdot)][M] \quad (2-2)$$

$$\frac{d[R\cdot]}{d\tau} = k'[(2R_c\cdot)][M] - k''[R\cdot][M] = 0 \quad (2-3)$$

$$\frac{d[M]}{d\tau} = -k'[(2R_c\cdot)][M] - k''[R\cdot][M] - k_p[M][RM\cdot] \quad (2-4)$$

$$\frac{d[RM\cdot]}{d\tau} = k'[(2R_c\cdot)][M] + k''[R\cdot][M] - 2k_t[RM\cdot]^2 = 0 \quad (2-5)$$

$$R_p = \frac{-d[M]}{d\tau} = k_p \left[ \frac{k'fk_d}{k_t} \right]^{1/2} [M]^{3/2} [I]^{1/2} \quad (2-6)$$

Several assumptions are made during these kinetic considerations, with the first one being that the reactions take place isothermally and are irreversible. The second assumption is that there is a constant fraction of caged radicals proportional to the decomposed initiator ( $[(2R_c\cdot)] = fk_d[I]$ ). The third assumption is that  $k_d[I] \gg k'[(2R_c\cdot)][M]$ , meaning that the rate at which the initiator decomposes into two caged free radicals is much faster than the rate at which the caged radicals are intercepted by the monomers. This is contrary to what is typical for FRPs, but it explains why the polymerization rate does not have a 1st power dependence on the monomer concentration<sup>14</sup>. Finally, a pseudo steady state assumption is made where  $[R\cdot]$  and  $[RM\cdot]$  get consumed as soon as they are generated, thus their concentrations remain constant, i.e. the net rate of Equations 2-3 and 2-5 are equal to zero. With all these assumptions in place, the final polymerization rate can be calculated as shown in Equation 2-6.

### 2.3 Rate Constants

Linear interpolation of Borisov's work (Table 1) at 90 °C leads to Equation 2-7, whereby the decomposition rate of APS can be estimated from the initial concentration of APS<sup>13</sup>. Borisov comments that at initial APS concentrations above 0.080 mol/L, the  $k_d$  values deviate from their linear trend<sup>13</sup>. Therefore, Equation 2-7 is only reliable for  $[APS]_0 \leq 0.080$  mol/L.

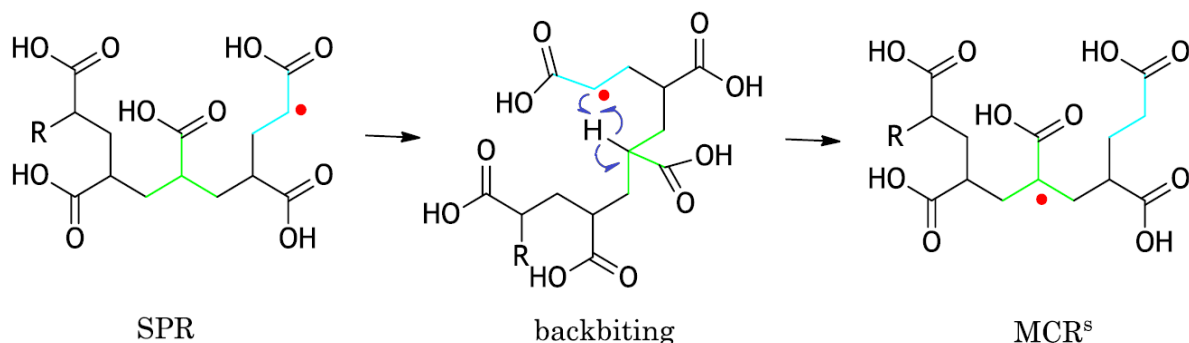
$$k_d = (-3 \times 10^7)[APS]_0 + (3 \times 10^6) \quad (2-7)$$

**Table 1: Borisov's APS rate constants as a function of initial concentration and temperature<sup>13</sup>**

$[APS]_0$ /mol L <sup>-1</sup>	$k_d \cdot 10^5/s^{-1}$			
	353 K	358 K	363 K	368 K
0.008	8.2±0.3	15.0±1.2	30.0±3.5	40.5±2.3
0.024	7.2±0.3	13.0±0.7	25.7±1.7	40.0±1.3
0.048	6.5±0.2	11.6±0.8	18.0±1.3	35.7±1.0
0.065	5.0±0.2	10.5±0.7	13.5±0.8	33.0±2.2
0.080	4.2±0.3	10.3±0.7	12.0±1.2	31.3±1.5
0.130	6.8±0.5	5.5±0.3	27.5±2.3	40.5±0.5
0.380	14.5±0.5	14.8±1.3	26.5±1.5	43.0±2.8
0.770	23.2±2.0	29.7±2.7	48.5±3.0	50.3±4.3

Regarding potential  $k_p$  values for AA in literature, Moad and Solomon explain that PLP-SEC (Pulsed Laser and Size Exclusion Chromatography Method) is the most reliable method for  $k_p$  determination but sometimes has difficulties with high  $k_p$  monomers such as acrylics (especially in aqueous solutions) due to "backbiting" (i.e., chain transfer) interference<sup>15</sup>. Backbiting is the incident in which a radical on the end of a growing polymer chain (secondary propagating radical, SPR) reacts with a hydrogen several bonds away from it on the same chain, making it so the radical and hydrogen switch places (Scheme 3)<sup>16,17</sup>. (This is specifically known as 1,5-hydrogen shift if the radical switches with the hydrogen five bonds away from it).

Backbiting changes the SPR into a more stable tertiary midchain radical (MCR) which causes an overall slower propagation rate. For this reason, lower reaction temperatures and dilute solutions are needed in order to obtain accurate  $k_p$  values.



**Scheme 3: Mechanism for 1,5- hydrogen shift backbiting by Wittenberg<sup>16</sup>**

Wittenberg has an excellent paper that collates prominent kinetics work from Lacík, Buback, Beuermann, Barth, and Moad and models the kinetics of FRP of AA<sup>15,17-20</sup>. Modified from Wittenberg, Equation 2-8 estimates  $k_p$  values of non-ionized AA based on monomer concentration  $[M]$  (mol/L) and temperature (K). ( $k_p^s$  indicates the  $k_p$  of end-chain (secondary propagating) radicals which are by far the most prominent at conversions lower than 97%)<sup>17</sup>. Non-ionized means that the AA solution has a degree of ionization equal to zero ( $\alpha = 0$ ) (i.e. no ionizing agent such as NaOH is present) and that  $\text{pH} \approx 2.0$ . The  $k_p$  of AA decreases as the concentration of AA increases; this agrees with literature<sup>19</sup>.

$$k_p^s = (3.2 \times 10^7) \exp\left(\frac{-1564}{T}\right) \cdot (0.11 + (0.89) \cdot \exp(-0.216 \cdot [M])) \quad (2-8)$$

Modified from Wittenberg, Equation 2-9 estimates  $k_t$  from initial monomer concentration,  $[M]_0$  (mol/L), temperature (K), and number average chain length ( $i_n$ )<sup>17</sup>. ( $k_t^{ss}$  is specifically the termination rate between two active chains with secondary propagating radicals, but these are the most common type of radicals).  $k_t$  decreases as the chain length grows due to

the difficulty that the free radical ends have in finding each other for termination, i.e. the increased viscosity at higher conversion makes termination diffusion-controlled.

$$k_t^{SS} = \left\{ \left[ (9.78 \times 10^{11}) \exp \left( \frac{-1860}{T} \right) \right] \cdot (1.56 - 0.127[M]_o - 1.2 \left( \frac{[M]_o}{13.89} \right)^2 + 2.43 \left( \frac{[M]_o}{13.89} \right)^3 \right\} \cdot (30^{-0.44}) \cdot (i_n^{-0.16}) \quad (2-9)$$

Calculated from Borisov and Wittenberg's equations, Table 2 approximates rate constant values for  $k_d$ ,  $k_p$ , and  $k_t$  at initial AA concentrations of 0.70 and 3.00 (mol/L), 90 °C, and two different MWs. These conditions are relevant to the research in this thesis.  $k_d$  is independent of starting AA concentrations.

**Table 2: Estimated rate constants at varying initial concentrations and 90 °C**

$k_d$ (1/s)			[AA] <sub>0</sub> (mol/L)	$k_p$ (L/mol s)	$k_t$ (L/mol s)	
[APS] <sub>0</sub> (mol/L)					7200 MW	300000 MW
0.056	0.068	0.112				
1.32 × 10 <sup>6</sup>	9.6 × 10 <sup>5</sup>	2.45 × 10 <sup>6</sup>	0.70	3.77 × 10 <sup>5</sup>	9.16 × 10 <sup>8</sup>	5.05 × 10 <sup>8</sup>
			3.00	2.48 × 10 <sup>5</sup>	7.15 × 10 <sup>8</sup>	3.94 × 10 <sup>8</sup>

### 3.0 Experimental Setup

#### 3.1 FlowSyn System and Additional Components

As seen in Figure 3, the custom FlowSyn instrument from Uniqsis provides two continuous HPLC pumps (Pump A and B), two regions of static mixing, and internal pressure readings. The pumps are 316 stainless steel with a mix of stainless steel and PTFE connections. Pump A and B both have 2.8 bar back pressure regulators installed (purchased from Idex).

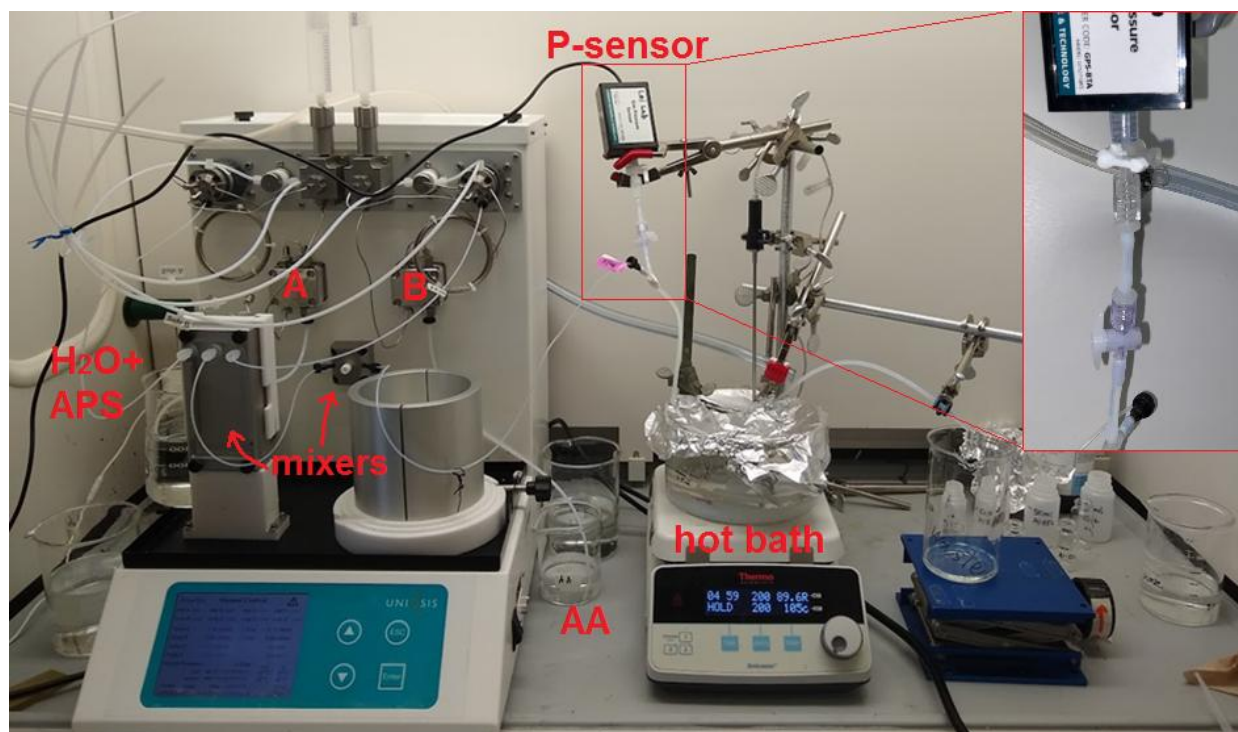


**Figure 3: FlowSyn setup for the continuous flow production of polyacrylic acid**

Each pump's ratings are for 50 mL/min, however, they are only able to accurately pump up to 31 mL/min each with a resolution of 0.05 mL/min. It is useful to note that new flowrates can be set ahead of time before initiating them. The glass chip static mixer has a total volume of 2 mL. The second static mixer (arrowhead) comes standard with each FlowSyn unit and is

combined with an internal pressure transducer for the system. Brocken et al. have previously demonstrated the FlowSyn's capabilities for continuous polymerization research at low initial concentrations<sup>5</sup>. The compact and simple nature of the FlowSyn instrument makes it ideal for investigating CF processes.

The easiest way to test different residence times (RT) is to simply change the flow rate. However, it is important to note that Qiu et al. did find that in their microreactor polymerization process, flow rates slower than 20 mL/min (from RTs of 0.3-3.5 min) did exhibit slightly lower % conversions<sup>6</sup>. They attributed this flow-rate variable conversion to poor mixing of the monomer and initiator<sup>6</sup>. Additionally, Bally et al. highlight the importance of good mixing in continuous flow systems that have fast exothermic reactions so the formation of hotspots and high molecular weight (MW) build up is mitigated<sup>21</sup>. These findings gave more impetus for why two static mixers are used in this research.

Due to polymer plugging problems, the traditional stainless steel FlowSyn coils are substituted with 1/8" inner diameter and 3/16" outer diameter PTFE tubing coiled in a water hot bath (170mm x 90mm Pyrex<sup>®</sup> dish from Corning) with magnetic stir bar and temperature maintained by a hotplate with attached thermocouple. The advantage of this tubing is that it can be easily replaced anytime permanent fouling occurs. An aluminum foil cover is placed over the hot bath to help keep consistent temperature and reduce water evaporation. The tubing and hotplate used are purchased from McMaster-Carr and Thermo Scientific. An additional (gas) pressure sensor from Vernier, placed before the hot bath, and air cooling, placed after the hot bath, have been added to the system. The Vernier pressure sensor is set up to collect one data point every 3 seconds and produce a live graph of the system pressure. It can be manually toggled to measure standard atmosphere (to get a baseline) or the system pressure before the

reaction zone. The maximum pressure it can sense is 210 kPa. The final polymer product is collected in 60 mL HDPE bottles from Fisher Scientific.

### **3.2 Chemicals**

The acrylic acid (99% pure with 200ppm MEHQ as an inhibitor), ammonium persulfate, and phenothiazene, were purchased from Sigma Aldrich and utilized as received. The sodium selenite was purchased from Alfa Aesar and is kept nearby as an emergency radical terminator.

### **3.3 General Lab Procedure**

The following procedure is for producing multiple samples of same concentrations and temperature but with varied residence times. The target flow rates and reservoir volumes are calculated based on desired initial monomer and initiator concentrations as well as total volume of tubing within the hot bath of a certain water level (reaction zone). The FlowSyn, hotplate, hot bath, air cooling, and tubing as well as DI water filled beakers for Pump A and B are set in place. The tubing is coiled in the hot bath a number of times needed for a targeted reaction zone volume which determines the magnitude of residence times to be tested. In general, a shorter reaction zone leads to the need for slower flow rates while a longer reaction zone allows for higher flow rates, or longer residence times. Primarily due to the small inner diameter, slightly low flow rates, and varying viscosity within this research, the Reynolds number ranges from  $2.7 \times 10^{-5}$  to 20.3. Since this is well below 2000, the flow is expected to be always laminar.

With luer-lock syringes, both FlowSyn pumps are primed using the DI water reservoirs (to remove any air in the pumps). Any liquid that comes in contact with the Vernier pressure gauge may damage it, thus a pocket of air is created between the pressure gauge and main tubing line by pumping DI water past the closed two-way valve while the T-junction valve is open to atmosphere. When it is closed off from atmosphere and open to the tubing, the pressure gauge can then monitor the system pressure continuously.

The DI water is pumped through the system at  $\sim 1$  mL/min while sample bottles and monomer/initiator reservoirs are prepared. Two beakers are used as reservoirs for a mix of DI water plus APS and neat AA, but surplus is added to prevent the pump inlets from getting close to sucking air (as the levels drain). The "DI water + APS" reservoir beaker is prepared in the correct proportion that will provide the desired APS concentration when added to neat AA (determined by flow rate ratios). The flow is stopped and the DI water reservoirs are substituted for the two chemical reservoirs: DI water + APS for pump A and neat AA for Pump B. Once again, the pumps are primed. The air cooling is turned on.

Once the hot bath is 92-93 °C, Pump B is started at 1.0 mL/min and  $\sim 2$  mL of AA are pumped into the system (up to the mixer chip). The purpose for this is to dispense the slower flow rate AA earlier into the system so mixing will occur from the start. Both pumps are then started with the desired flow rates for the first sample to be collected. The target temperature is typically 90 °C and the faster residence time samples are run first. The faster flow rate of room temperature fluid typically lowers the hot bath temperature by 2-3 °C. Also, it is easier to cool the system than to heat it, so aiming for a slightly higher temperature is helpful.

The first 50-90 mL of polymer are rejected as the system needs time to have both reservoirs start mixing (at their respective flow rates); this volume is several times larger than the

volume of the reaction zone. For each sample, ~50 mL are collected and flow rates for the next sample are set and started, then ~40 mL are rejected before collection begins again. To maintain a consistent baseline and to protect the pressure gauge from any unforeseen pressure spikes, the Vernier pressure gauge is closed from the system and opened to atmosphere before new flow rates are started. About one minute after changing the flow rate, the gauge is returned to measuring the system pressure.

When fully collected, each sample is placed into an ice bath to reach near room temperature or colder; faster residence time samples tend to be hotter, possibly due to lingering exothermic reactions with any unreacted monomers still present. Figure 4 shows a 1-minute residence time PAA sample, with initial AA and APS concentrations of 3.00 and 0.068 mol/L respectively. This particular sample was boiling right after collection.



**Figure 4: PAA boiling immediately after sample collection**

An accurate hot bath water level must be maintained by occasionally adding hot water (without cooling the bath too much). When there is time between sample collections, ~0.001g of phenothiazene (PTZ) is mixed into each polymer sample. The purpose of PTZ is to scavenge any

remaining free radicals to prevent further polymerization of any unreacted monomer. Via a catalytic process, PTZ is capable of trapping two radicals per molecule and is only consumed due to side reactions like oxidation<sup>22</sup>.

It is useful to clean the system while it is still hot. To start cleaning (while the system is still running), both (nearly empty) reservoirs are diluted with DI water and both pumps are turned to a flow rate of ~3 mL/min for about 5 minutes (with waste beaker as collection). Then the reservoirs are diluted again and pumped for another 5 minutes. The pumps are paused and both reservoirs are replaced with neat DI water. The pumps are primed again to rinse their internals with the water and remove any potential air bubbles (from switching the reservoirs), then pumping continues for 10 minutes. The flow rate is changed to 25 mL/min for each pump which are pumped for 1 minute. The flow is stopped, the pressure gauge is closed off from the system, the tubing is moved from 'after the pressure transducer' to the air hose, and air is blown through the tube to push out all the water. The tube is then closely inspected for any fouling as seen in Figure 5. If any fouling is present, the tube is discarded. Fouling commonly occurs at long residence times ( $RT \geq 4$  min) and/or higher concentrations ( $[AA]_0 \geq 1.40M$ ). The AA, APS, and waste beakers are rinsed several times with water and wiped clean.

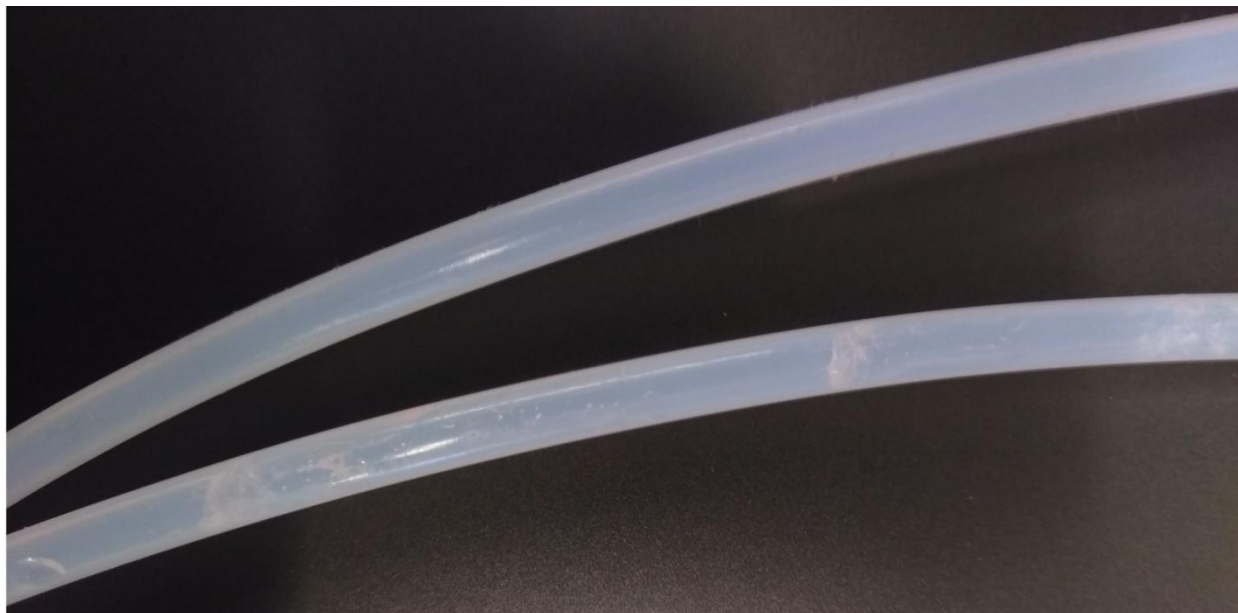


**Figure 5: Clean PTFE tube (top) compared to tube with polymer fouling (bottom).**

### **3.4 Sample Characterizations**

All characterizations in this research have been conducted by Lubrizol. The molecular weights of the products were determined by GPC (gel permeation chromatography) Waters 515 pump with 717plus auto-sampler and 2414 RI Detector (40°C) (Figure 6). In Figure 6, the top graph is the GPC signal vs retention time. The polymers with the highest MW elute out first while the polymers with the lowest MW elute out last. The bottom graph presents a logM distribution plot of the molecular weight averages for the distribution. The flow was 0.7 mL/min, the mobile phase was 0.1 M aqueous sodium nitrate solution, the column was TSKgel Guard with 2x TSKgel GMPWxl (300 x 7.8 mm). The weight and number average MWs were calculated based on NaPAA standards and are used to calculate the polydispersity index (PDI).

The residual AA was determined by high-performance liquid chromatography (HPLC) with a Phenom Luna 18(2) column (4.6x150mm, 5um) with a run time of 30 minutes. The %solids was determined by the sample first being heated to 25 °C via hot bath then being dispersed on a glass fiber pad. After this, the sample had its weight difference before and after microwaving at 30% power for 10 seconds measured.

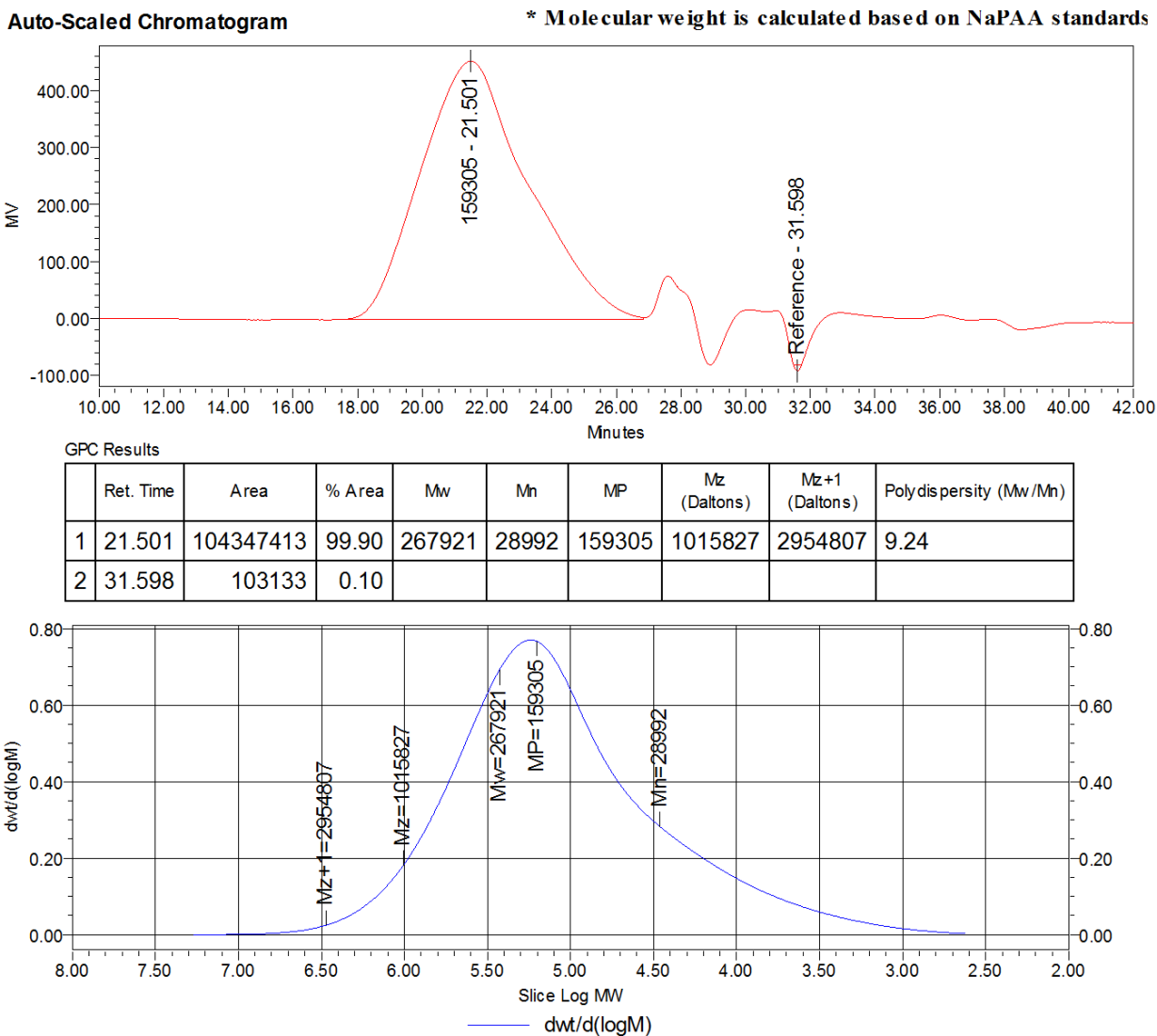


**Figure 6: GPC data for sample of  $[M]_0 = 2.92$ ,  $[I]_0 = 0.077$  and 2 minute residence time provided by Lubrizol**

## 4.0 Results and Discussion

In this research, the temperature was fixed at 90 °C while the initial monomer (AA) and initiator (APS) concentrations were varied, (0.70-3.00 M and 0.056-0.112 M respectively). The samples were collected over a range of residence times (RT). When analyzing the general trends discovered (Figures 7-9), several relationships between the parameters become evident as summarized in Table 3. The "early cooling" sample was immediately chilled in an ice bath after coming out while the other samples were cooled in an ice bath after 50 mL were collected. The target values of different parameters were: molecular weight (MW) = 300,000 g/mol, polydispersity index (PDI) = 10, % Solids= 25%, and AA conversion  $\geq$  99.0%; the red dashed lines in Figures 7-9 indicate these target specifications. The trend highlighted in red in Table 3 indicates that the initial concentration of initiator strongly affects MW, PDI, and % monomer conversion. The pH for all runs ranged from 1.7-2.3 with 1.96 being the average. In this research, pH decreased with increasing initial monomer concentration.

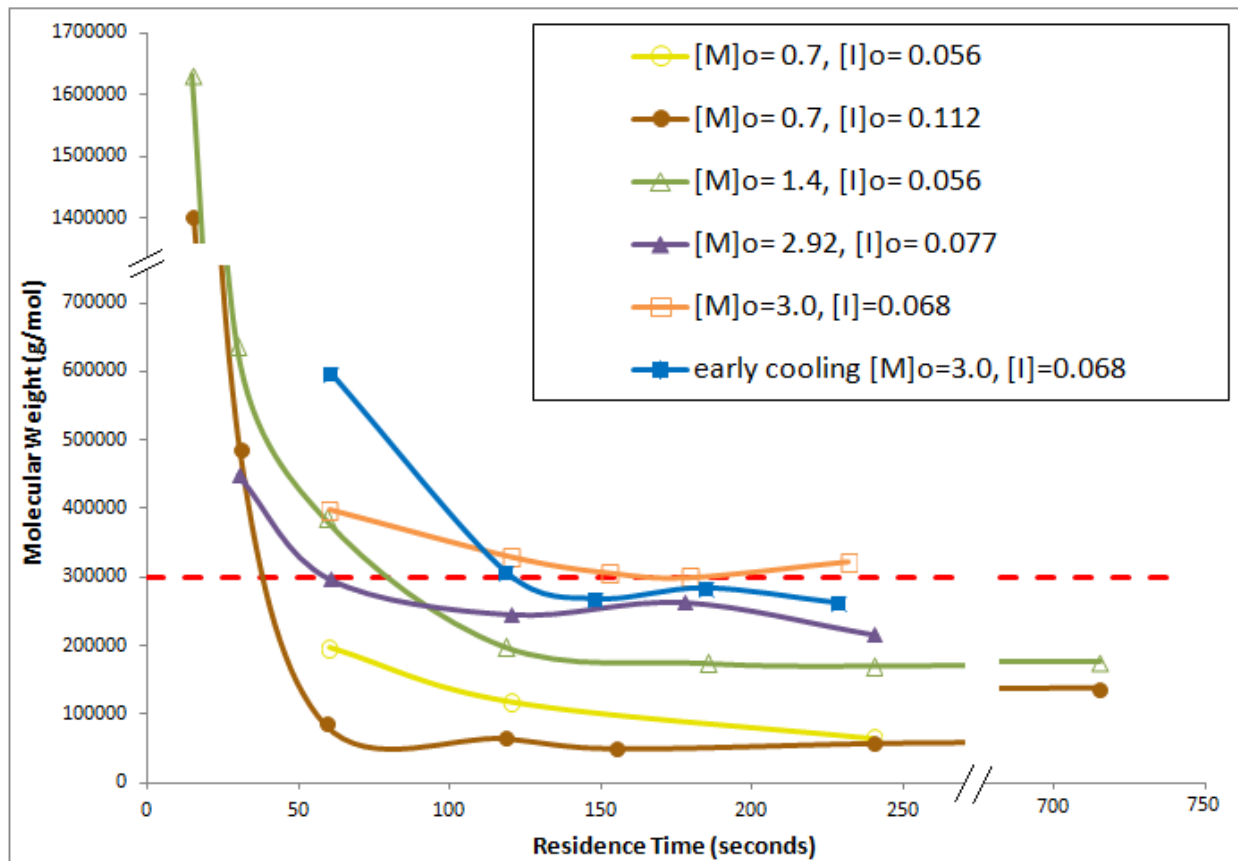


Figure 7: PAA product molecular weight with residence time at various initial concentrations.

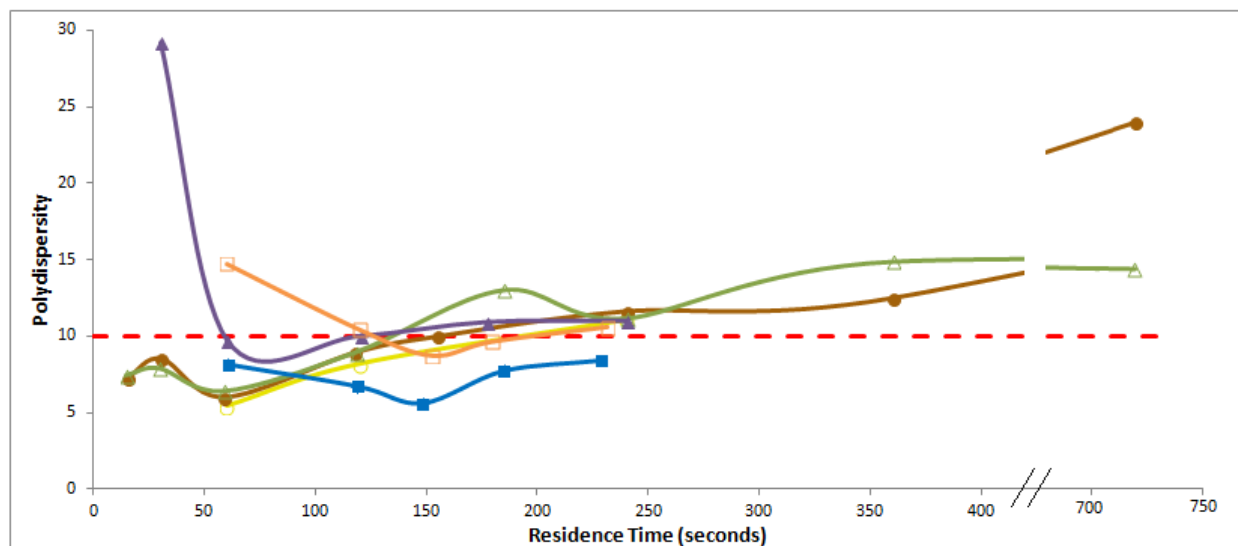


Figure 8: PAA product polydispersity with residence time at various initial concentrations.

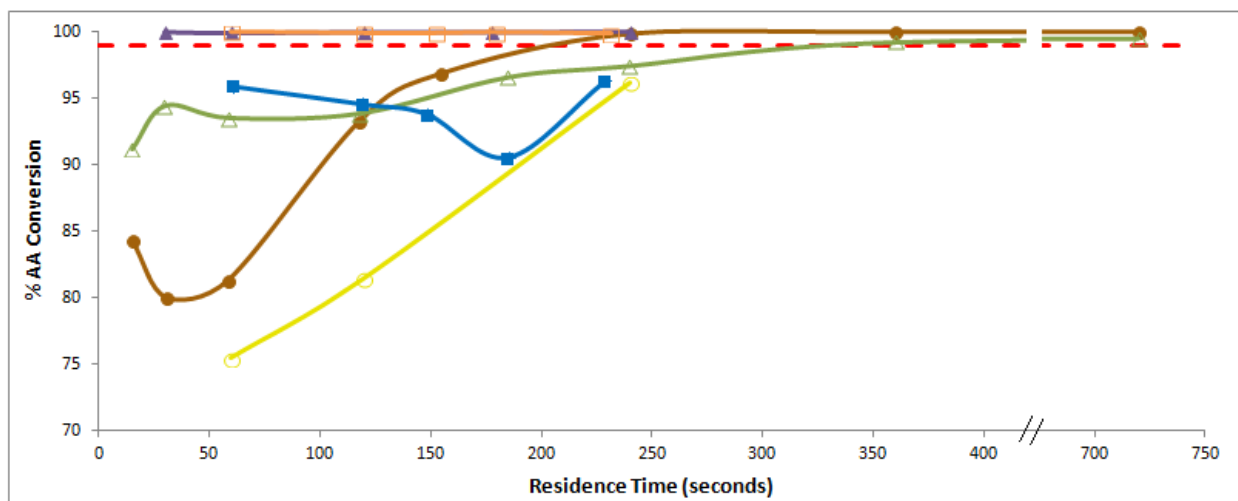


Figure 9: PAA product % monomer conversion with residence time at various initial concentrations.

Table 3: General trends when increasing residence time, and initial monomer and initiator concentrations.

<u>Increasing...</u>	<b>MW</b>	<b>PDI</b>	<b>% [M] conversion</b>
<b>[M]<sub>o</sub></b>	Increase	-----	Increase
<b>[I]<sub>o</sub></b>	Decrease	Increase	Increase
<b>Residence Time</b>	Decrease	Increase	Increase

As previously mentioned, at higher initial AA concentrations, faster RT samples (RT ≤ 2 min) would come out extra hot, sometimes to the point of boiling. This indicates that there still is a significant amount of unreacted monomer present, which still take part in the highly exothermic polymerization reactions after leaving the reaction zone, extending the RT. This means that the actual conversion should be lower than reported values.

As indicated by the asterisks in Appendix Table 1, several data points were averaged between two runs. These points were repeated to test the reproducibility of the experiment. Additionally, to check the consistency of product produced over an extended period of time, one experiment maintained consistent starting concentrations (  $[M]_o = 1.4$  &  $[I]_o = 0.056$  mol/L ), residence times (1.19 min), and temperatures (90 °C) while samples were collected over a range

of 8 hours (Figure 10). This demonstrates that there is a decrease in both MW and % conversion performance as product is produced over longer periods of time. The reason for this is not known at this point. One possibility is that polymer fouling of the reaction tubing, which was observed in this run, builds up on the tubing walls overtime, leading to a reduction in the residence time and heat transfer effectiveness. With less heat, % monomer conversion decreases. As seen in Figures 7-9, the target specs were closely met with the ~3 minute RT samples of  $[M]_o = 2.92$   $[I]_o = 0.077$  and  $[M]_o = 3.0$   $[I]_o = 0.068$  mol/L.

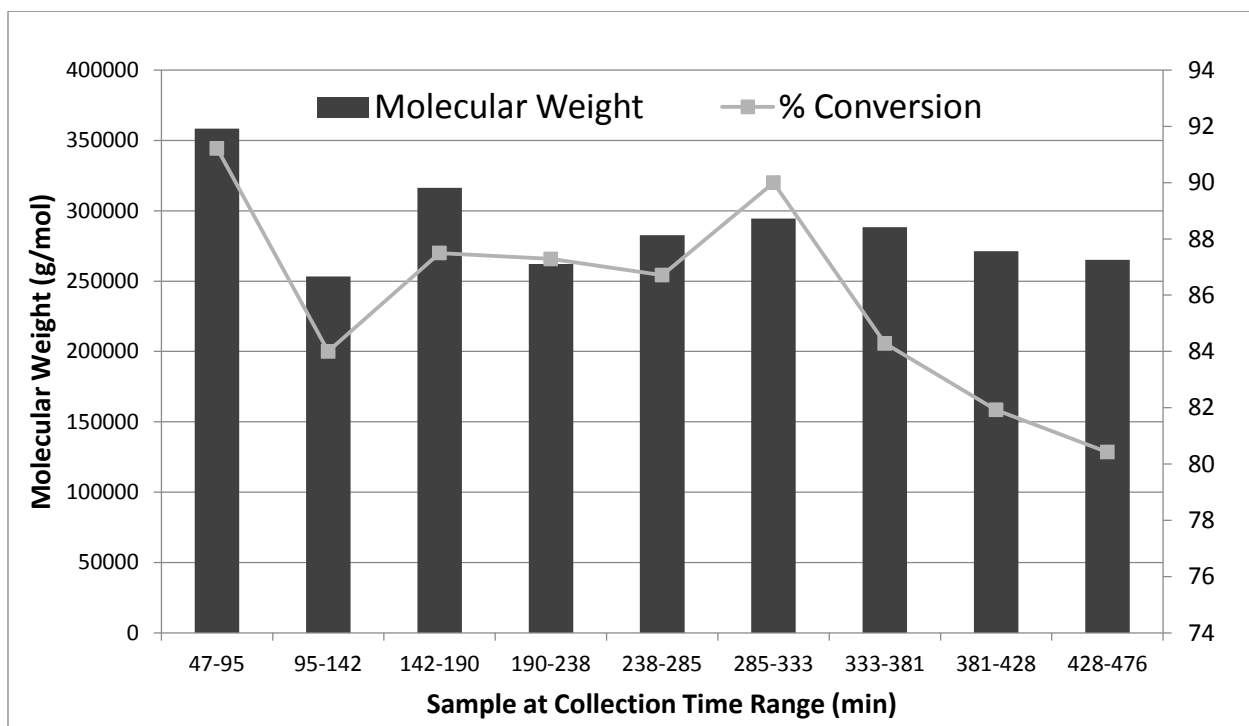


Figure 10: MW and % conversion over 8 hour period of sample collection

## 4.1 Effect of Different Parameters

### 4.1.1 Initial Monomer Concentration

An increase in the initial monomer concentration increases the average chain length, which in turn increases the MW. Equation 4-1 shows the kinetic chain length for PAA. Since the propagation rate ( $R_p$ ) has a higher dependence on monomer concentration (as previously discussed in Section 2.2, Equation 2-6), the kinetic chain length will also share that dependence. A higher initial monomer concentration also increases monomer conversion; this was clearly seen in the experiments (Figure 9) and agrees with literature for AA FRP (Figure 1)<sup>6,14</sup>. As previously mentioned, this conversion vs time dependence on initial monomer concentration is likely due to the increased presence of monomers that are available to interact with free radicals that are trapped in solvent cages.

$$\bar{\nu} = \frac{R_p}{r_d} = \frac{k_p(k')^{\frac{1}{2}}[M]^{\frac{3}{2}}}{(k_t k_d f[I])^{\frac{1}{2}}} \quad (4-1)$$

Additionally, a higher starting monomer concentration naturally means higher percent solids in the final product (less dilute). This is important, as "shipping water" is expensive in industry and evaporating water from the final product without affecting its quality may not be viable. Initial monomer concentration seems to have little to no effect on PDI.

### **4.1.2 Initial Initiator**

An increase in the starting initiator concentration increases the amount of free radicals. This leads to a higher polymerization rate and lower MW (because more shorter chains are being produced (initiated and terminated) (Equation 4-1)). An increase in the initial initiator concentration also increases AA conversion because more free radicals are available to react with AA monomers. However, with more initiator, the PDI increases. The reason for this is not understood, but more radicals being present during polymerization could lead to a larger diversity in molecular weights.

### **4.1.3 Residence Time**

AA conversion and PDI increase when the residence time is increased because there is more time for reactions to occur (and average MW to become distributed). Additionally, at longer RTs, the MW is decreased. The reason for this is not clear, but it is suspected that (in the current laboratory set up) shorter residence times (high flow rates) still leave a significant fraction of unreacted monomer while the fluid heats up from the natural exothermic reaction. In the presence of this heat, the reaction continues, even after the fluid leaves the heated zone and enters an ice bath. At longer residence times, the MW seems to stabilize.

The influence of the flow rate (with all other variables held constant) has not been tested, however the system does have two static mixers to ensure adequate mixing.

#### 4.1.4 Temperature

The influence of temperature on final PAA properties has only lightly been investigated. Table 3 compares three samples with the same initial concentrations but varying temperatures. (The 90 °C sample has a residence time of 12 minutes instead of 11 minutes and a slower flow rate, but it should still be comparable). It was found that that a higher temperature decreases MW and increases the PDI. The reason for this might be that a higher temperature will increase  $k_d$  much more than  $k_p$ <sup>10</sup>, which would ultimately decrease the kinetic chain length (Equation 4-1), i.e. decompose the initiator into free radicals faster and cause the formation of shorter chains. Table 4 indicates that increasing the temperature has very similar effects to that of increasing the initial initiator concentration.

**Table 4: PAA products at same initial concentrations but at different temperatures**

Conditions					Characterizations			
[AA] <sub>o</sub> (mol/L)	[APS] <sub>o</sub> (mol/L)	RT (min)	FR (mL/min)	Temp (°C)	MW (g/mol)	PDI	% Solids	% AA Conv.
1.4	0.056	11	1.55	65	942041	7.9	10.5	90.4
1.4	0.056	11	1.55	80	348713	12.1	11.3	98.2
1.4	0.056	12	1	90	177136	14.4	11.6	99.5

#### 4.1.5 Polydispersity Index

This research does not have a model on the nature of the PDI and how it changes based on conditions. PDI is the ratio of the mass-average molar mass to the number-average molar mass and a larger PDI indicates a broader spectrum of different molecular weight polymers in the mix. Different chain lengths arise from the balance between the rate of propagation and rate of termination<sup>23</sup>. Thus, any kinetic effects on these two rates will vary the PDI. At the start of

polymerization, high molar-mass polymers are generally formed<sup>23</sup>. Iwasaki did report that the improved heat transfer of CF polymerization strongly reduced the PDI of highly exothermic FRPs when compared to batch processes<sup>24</sup>. They suspected that this was due to a more consistent local temperature throughout the whole reaction zone. The Trommsdorff-Norrish gel effect, whereby localized viscosity increases slow termination reactions, could impact PDI, but Wittenberg comments that this effect is weaker in AA polymerizations compared to other FRP monomers such as methacrylic acid<sup>16</sup>.

## 4.2 Tube Fouling

The first several PAA products of this research were produced at lower initial monomer concentrations ( $[M]_o = 0.7$  and  $1.4$  mol/L). However, to meet target specifications, higher concentration products were produced as well ( $[M]_o = 2.92$  and  $3.00$  mol/L). Polymer fouling was encountered during two runs at  $0.70$  mol/L, several runs of  $1.4$  mol/L, and all runs of  $2.92$  and  $3.0$  mol/L of initial monomer. Regarding one of the runs at  $[M]_o = 0.70$ , the system tubing was actually in a  $1$  mm inner diameter stainless steel coil, and the heating and flow was stopped before the tubing was properly cleaned. This gave enough time for the monomer to polymerize and build up a viscous blockage. The other low concentration run showed a small build up of high MW polymer on some parts of the tube walls. PAA fouling appears as opaque streaks (on the wall) where the liquid flow passes through the middle (Figure 5). During high concentration runs, the fouling build up can be so great that full blockages occur.

As previously discussed in Section 2.3, chain transfer (backbiting) leads to radicals in the middle of a growing polymer chain (MCRs). According to Wittenberg, termination with these

radicals leaves branches in the final polymer<sup>17</sup>. MCRs become more prominent at higher conversions and especially at conversions greater than 97%. These branches are often only two monomer units long, but there is a possibility that branching increases the viscosity as well as the capabilities for gelling, and thus fouling to occur.

Towards the end of this research, a Vernier pressure gauge was installed so fouling could be monitored in real time. As indicated in Figure 11, there is a strong and steady pressure increase associated with increased fouling. Each pressure spike, such as the one at 38 minutes, is followed by a small blob of higher MW polymer being pushed out through the system. The pressure builds up until the foulant is dislodged, then it returns back (slightly higher as more semi-permanent fouling continues to gradually build up). Caution needs to be taken as these chunks of high MW polymer will end up being collected in the samples.

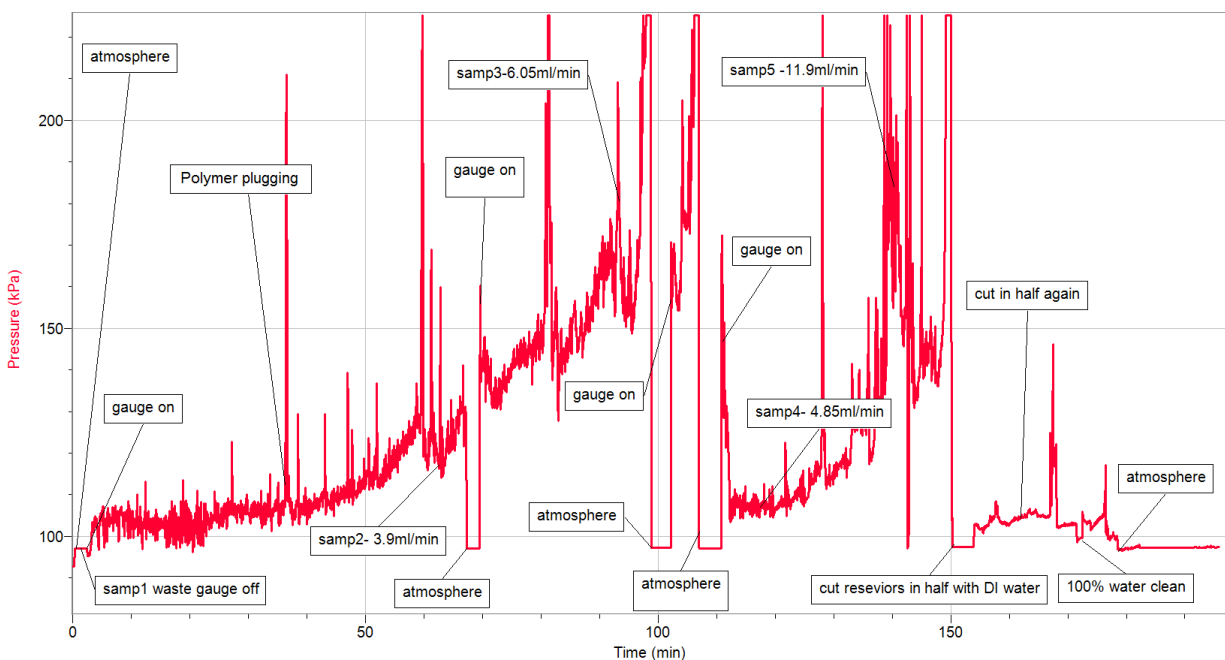


**Figure 11: Vernier pressure reading of high monomer concentration (3.0 M) polymerization run**

At 110 minutes of operation, the system partially "reset" itself by dislodging a majority of the stuck polymer. This stuck polymer then discharged out of the end of the tube as a constant

high MW string (Figure 12). In Figure 11, the ~97 kPa "atmosphere" pressure dips are when the pressure gauge was manually closed from the system and opened to atmosphere in order to protect it from high pressure and to measure the atmospheric baseline.



**Figure 12: String of previously stuck polymer extruding out**

### 4.3 Simulation

For this research, a simple simulation of the polymerization kinetics (as previously discussed) of AA with APS was created using MATLAB (Figure 13). In Figure 13, the left graph has initial monomer and initiator concentrations of 0.70 and 0.056 mol/L, respectively, and the right graph has 3.0 and 0.068 mol/L, respectively. The Y-axis is the concentration of a particular species normalized by the initial monomer concentration and the X-axis is the residence time in minutes. The purple line represents the current monomer concentration, the blue represents the current initiator concentration, the red dotted line represents the concentration of two caged radicals, the yellow dashed line represents the concentration of the free-range radicals, and the green dash-dotted line represents the current concentration of active radical chains.

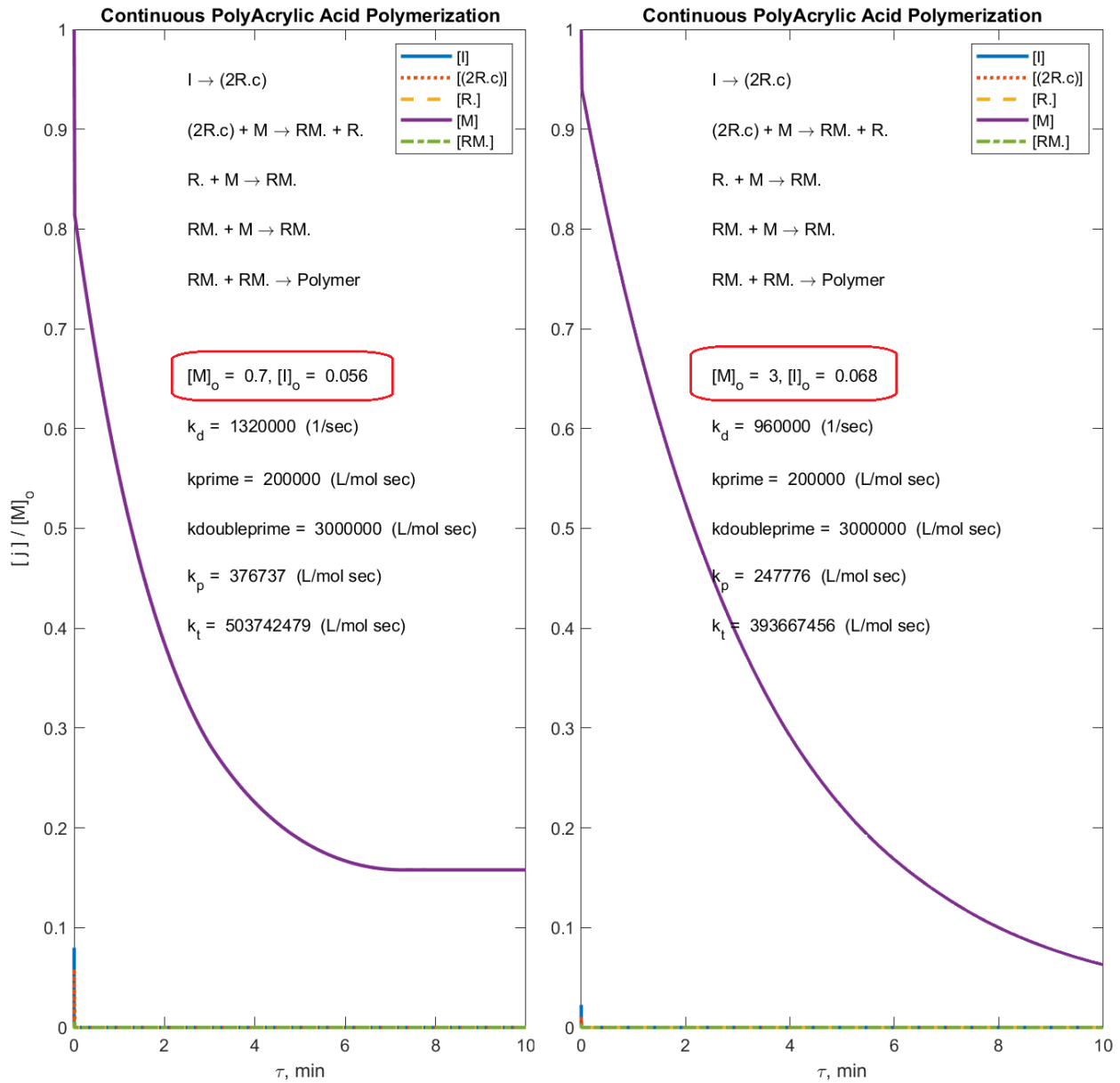


**Figure 13: MATLAB simulation for polymerization of AA with APS at low and high  $[M]_0$**

The estimated values for the rate constants  $k_d$ ,  $k_p$ , and  $k_t$  were calculated as shown in Table 2.  $k'$  and  $k''$  values were still unknown, and thus arbitrarily picked based on the roles of their reaction rates. As previously stated, it is assumed that  $k_d[I] \gg k'[(2R_c \cdot)][M]$ , so  $k_d$  should be much greater than  $k'$ .  $k''$  and  $k_p$  values should be high because they both involve typical fast radical attacks. All rate constants increase with increasing temperature.  $k_d$  changes

based on  $[I]_0$  and is related to the ionic strength of the solution<sup>13</sup>. In this simulation,  $k'$  and  $k''$  values are not changed because they are roughly estimated values.

Eighteen different simulation graphs with concentrations ranging from  $[M]_0$  of 0.7-2.8 and  $[I]_0$  of 0.056-0.224 mol/L and two temperatures of 80°C and 90°C were examined (Appendix Figure 2); the effects of temperature are seen by a change in the temperature dependent rate constants. As can be noticed in Figure 13, monomer consumption is very rapid in the beginning of the reaction, and then it decreases with time. Figure 14 shows the concentrations of the other components during this initial phenomenon at 90°C,  $[M]_0 = 0.70$ , and  $[I]_0 = 0.056$ . All  $[I]$  is consumed when only ~6%  $[M]$  has been consumed, and nearly all  $[(2R_c \cdot )]$ ,  $[R]$ , and  $[RM.]$  are consumed when ~18%  $[M]$  has been consumed. From this point, the system struggles to consume monomer and  $[M]$ 's consumption rate decreases with time. A probable reason for this is that the extremely large termination rate constant,  $k_t$ , has  $[RM.]$  getting consumed before  $[RM.]$  has a chance to keep reacting with further monomers. When the  $k_t$  is dropped by two orders of magnitude, ~50% of  $[M]$  becomes consumed before the other concentrations are depleted (and the line curves).

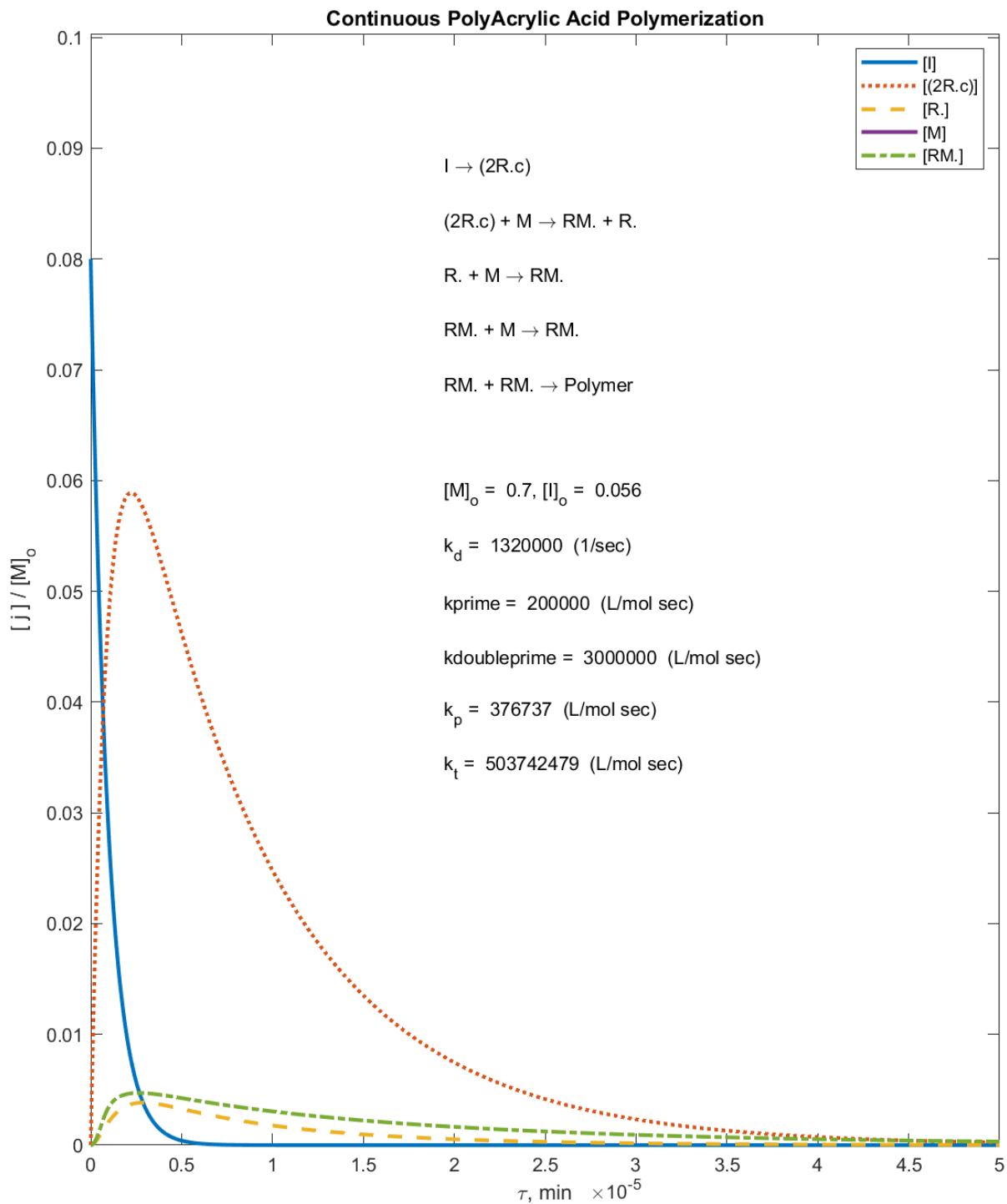


**Figure 14: Zoomed in view of [I], [(2R<sub>c</sub> ·)], [R ·], and [RM ·], at 90°C, [M]<sub>0</sub> = 0.7 and [I]<sub>0</sub> = 0.056 mol/L at very short RT**

Regarding the simulation, when the initial monomer concentration is increased from 0.7 to 1.4 mol/L, monomer conversion is improved, but when increased from 1.4 to 2.9 mol/L, the

improvement to conversion is negligible. When the initial initiator concentration is increased, the rapid consumption of [M] continues until more conversion is reached before the graph curves. However, increasing  $[I]_0$  does not increase the final conversion (Appendix Figure 2) which does not agree with observed trends. It seems that when the  $[I]/[M]$  ratio is too high, (also considering the increased [I] effectiveness at higher temperatures), the [M] conversion becomes extremely slow (nearly horizontal) after all the initiator is consumed. When not accompanied by the high  $[I]/[M]$  ratio, increasing the temperature only shows a very minor improvement to monomer conversion, which does not agree with observed trends. Interestingly, the simulation of  $[M]_0 = 1.4$  and  $[I]_0 = 0.224$  at  $90^\circ\text{C}$  was an outlier to some trends and had the best monomer conversion (near 100%) after a 10 minute residence time.

This simulation is in its early stages and does not yet account for all the specific details that Borisov's equations and Wittenberg's models have included<sup>13,16,17</sup>. Even though incomplete, the visual nature of this simulation could help reinforce current knowledge about FRP kinetics. A more robust simulation would provide support to future experiments by accurately predicting final polymer properties based on initial conditions. Ideally, a complete simulation could accurately predict final product MW.

## 5.0 Conclusion

This research has closely met target industrial parameters via a continuous flow tubular reactor, demonstrating that production of quality PAA is possible on this lab scale. However, as indicated by a constant pressure increase and physical evidence, the fouling that occurs at high monomer concentrations makes longer product collection times unreliable. The pseudo steady state kinetics and rate constants of free radical AA polymerization were reviewed and calculated. Experimental results agree with past reports that conversion increases with initial monomer concentration and that the polymerization rate has a  $3/2$  power dependence on monomer concentration. The general trends of changing the concentrations of AA and APS as well as the residence time were investigated and qualitatively determined.

From these kinetics, the starting framework of a simulation was created. Further evaluation and implementation of kinetic details are needed to improve this simulation. The feasibility of producing higher concentration PAA via a continuous reactor on a plant scale without being hindered by fouling remains to be investigated. If deemed viable, a continuous reactor for the production of PAA would create a more cost effective, safer, and potentially easier to manage process.

## 6.0 Future Work

In light of fouling of the reaction tube with polymer (especially at higher AA concentrations), more data and techniques to reduce fouling need to be established. Fouling poses a prevalent challenge to the industrial feasibility of producing high concentration PAA via a continuous flow tubular reactor. The consistency and accuracy of future data can be improved through the implementation of stronger temperature quenching. Additionally, the kinetic rate constants  $k'$  and  $k''$  are still yet to be determined. With further evaluation of kinetics from recent articles, a more robust simulation would be able to further guide future adjustments to the continuous operation. Additionally, it would be immensely valuable if the simulation could be used to predict product molecular weights based on all other parameters.

## Appendix A

$$A: \frac{d[I]}{d\tau} = -fk_d[I]$$

$$B: \frac{d[2R_c]}{d\tau} = fk_d[I] - k'[(2R_c)][M]$$

$$C: \frac{d[R\cdot]}{d\tau} = k'[(2R_c)][M] - k''[R\cdot][M] = 0$$

$$D: \frac{d[M]}{d\tau} = -k'[(2R_c)][M] - k''[R\cdot][M] - k_p[M][RM\cdot]$$

$$E: \frac{d[RM\cdot]}{d\tau} = k'[(2R_c)][M] + k''[R\cdot][M] - 2k_t[RM\cdot]^2 = 0$$

$$\frac{d[RM\cdot]}{d\tau} = 2k'fk_d[M][I] - 2k_t[RM\cdot]^2 = 0$$

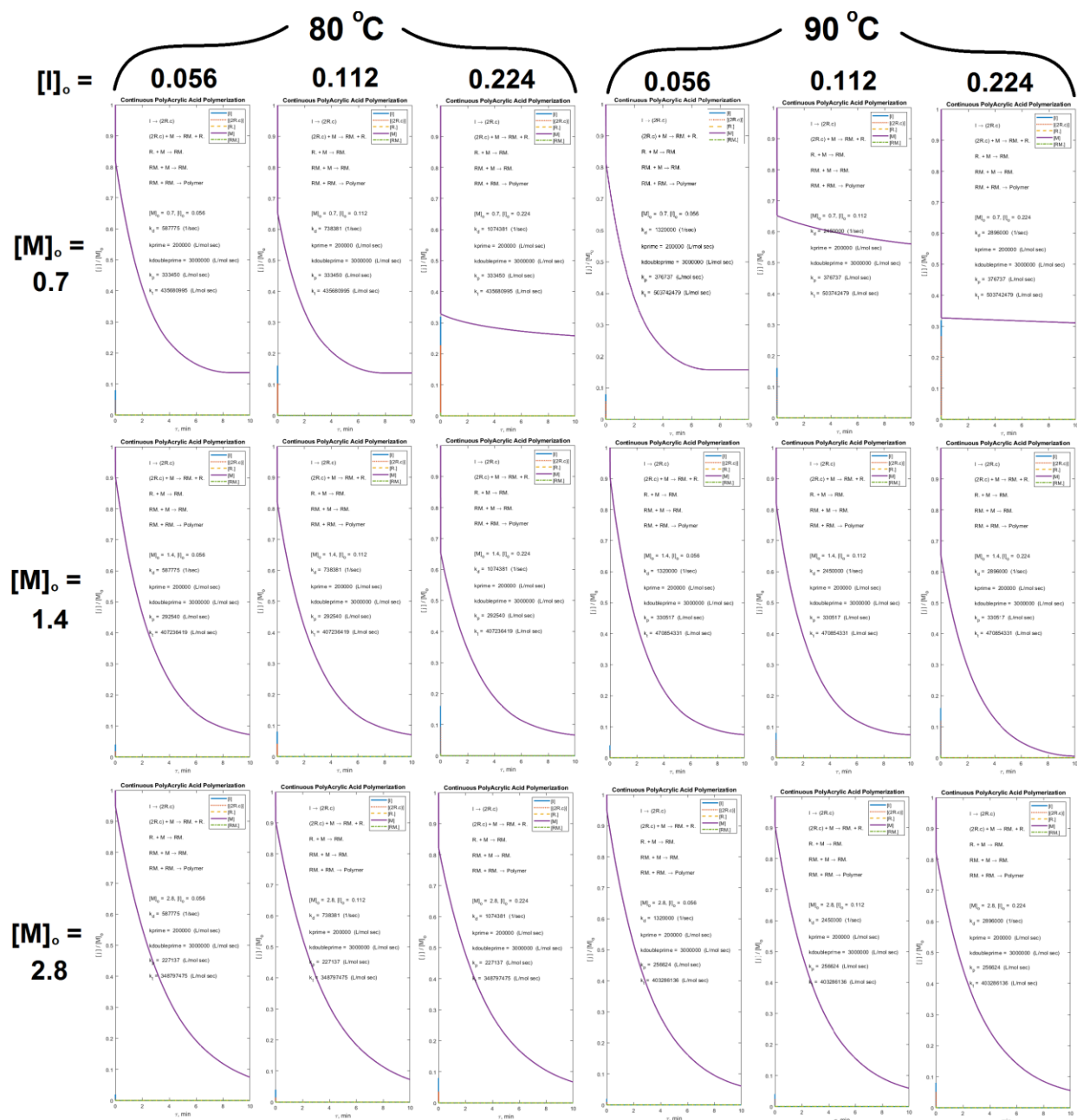
$$[RM\cdot] = \sqrt{\frac{k'fk_d[M][I]}{k_t}}$$

$$R_p = k_p[M][RM\cdot]$$

$$R_p = k_p[M] \left[ \frac{k'fk_d[M][I]}{k_t} \right]^{1/2}$$

$$R_p = \frac{-d[M]}{d\tau} = k_p \left[ \frac{k'fk_d}{k_t} \right]^{1/2} [M]^{3/2}[I]^{1/2}$$

Appendix Figure 1: Additional calculation steps for final polymerization rate



Appendix Figure 2: 18 simulation graphs depicting monomer consumption rate at different parameters over 10 min RT.

Appendix Table 1: All data used for Figures 7-9.

Conditions				Characterizations			
[AA]o (mol/L)	[APS]o (mol/L)	RT (Sec.)	FR (mL/min)	MW (g/mol)	PDI	% Solids	% AA Conv.
0.7	0.056	60	10	196790	5.4	5.1	75.4
		120	5	118502	8.2	6.0	81.4
		240	2.5	65545	11.0	5.4	96.1
0.7	0.112	15.36	31.2	1402873	7.3	4.4	84.3
		30.6	15.65	485554	8.5	6.3	80.0
		58.8	10.15	85336.5	6.0	7.0	81.3 *
		117.9	5.075	64753.5	8.9	7.6	93.3 *
		154.8	3.1	50080	10.0	7.4	96.9
		240	3	57742	11.6	7.6	99.9
		360	2	67927	12.5	7.6	100.0
		720	1	140235	23.7	7.5	100.0
1.4	0.056	14.86	32.3	1632526	7.5	11.6	91.1
		29.72	16.15	637547	7.9	11.2	94.4
		58.74	10.175	385757	6.4	10.5	93.5 *
		117.9	5.075	198915	8.9	11.1	93.8 *
		184.8	2.6	174166	13.0	11.5	96.6
		240	3	170252	11.2	11.5	97.4
		360	2	175117	14.9	11.6	99.2
		720	1	177136	14.4	11.6	99.5
2.92	0.077	30	32	449248	29.2	24.1	100.0
		60	16	298027	9.7	24.1	99.9
		120	8	245870	10.0	23.6	100.0 *
		177.3	5.415	263641	10.9	23.9	100.0
		240	4	216475	11.0	23.3	100.0
3	0.068	60	16	398185	14.8	23.8	100.0
		120	8	330216	10.4	24.0	99.9
		152.4	6.3	307054	8.7	23.4	99.9
		179.4	5.35	300595	9.6	23.7	99.9
		231.6	4.15	323256	10.6	23.6	99.8
3**	0.068**	60.6	11.9	597145	8.2	23.1	95.9
		118.8	6.05	306511	6.8	23.5	94.6
		148.2	4.85	268458	5.6	22.1	93.8
		184.8	3.9	284345	7.8	22.1	90.5
		228.6	3.15	262545	8.5	22.7	96.3

## Bibliography

- [1] Fitzpatrick, D. E., Battilocchio, C., & Ley, S. V. (2016). Enabling Technologies for the Future of Chemical Synthesis. *ACS Cent Sci*, 2(3), 131-138. doi:10.1021/acscentsci.6b00015
- [2] Tonhauser, C., Natalello, A., Löwe, H., & Frey, H. (2012). Microflow Technology in Polymer Synthesis. *Macromolecules*, 45(24), 9551-9570. doi:10.1021/ma301671x
- [3] Illg, T., Lob, P., & Hessel, V. (2010). Flow chemistry using milli- and microstructured reactors-from conventional to novel process windows. *Bioorg Med Chem*, 18(11), 3707-3719. doi:10.1016/j.bmc.2010.03.073
- [4] Watts P, Wiles C. Micro Reactors, Flow Reactors and Continuous Flow Synthesis. *Journal of Chemical Research*. April 2012:181-193. doi:10.3184/174751912X13311365798808
- [5] Brocken, L., Price, P. D., Whittaker, J., & Baxendale, I. R. (2017). Continuous flow synthesis of poly(acrylic acid) via free radical polymerisation. *Reaction Chemistry & Engineering*, 2(5), 662-668. doi:10.1039/c7re00063d
- [6] Qiu, L., Wang, K., Zhu, S., Lu, Y., & Luo, G. (2016). Kinetics study of acrylic acid polymerization with a microreactor platform. *Chemical Engineering Journal*, 284, 233-239. doi:10.1016/j.cej.2015.08.055
- [7] Mandity, I. M., Otvos, S. B., & Fulop, F. (2015). Strategic Application of Residence-Time Control in Continuous-Flow Reactors. *ChemistryOpen*, 4(3), 212-223. doi:10.1002/open.201500018
- [8] Serra, C., Schlatter, G., Sary, N. et al. Free radical polymerization in multilaminated microreactors: 2D and 3D multiphysics CFD modeling. *Microfluid Nanofluid* 3, 451-461 (2007). <https://doi.org/10.1007/s10404-006-0130-7>
- [9] Begall, M., Krieger, A., Recker S., Herbstritt, F. et al. Reducing the Fouling Potential in a Continuous Polymerization Millireactor via Geometry Modification. *Industrial & Engineering Chemistry Research* 2018 57 (18), 6080-6087 DOI: 10.1021/acs.iecr.8b00206
- [10] Cowie, J. M. G., Arrighi V., (2007). *Polymers: Chemistry and Physics of Modern Materials* (third edition). ISBN: 978-0-8493-9813-1
- [11] <https://chem.libretexts.org>
- [12] <https://polymerdatabase.com>

- [13] I. M. Borisov, R. S. Luksha, S. T. Rashidova, Kinetic features of ammonium persulfate decomposition in aqueous medium. *Russian Chemical Bulletin* 2015, 64, 2512-2513.
- [14] Cutié, S.S., Smith, P.B., Henton, D.E., Staples, T.L. and Powell, C. (1997), Acrylic acid polymerization kinetics. *J. Polym. Sci. B Polym. Phys.*, 35: 2029-2047. [https://doi.org/10.1002/\(SICI\)1099-0488\(19970930\)35:13<2029::AID-POLB4>3.0.CO;2-R](https://doi.org/10.1002/(SICI)1099-0488(19970930)35:13<2029::AID-POLB4>3.0.CO;2-R)
- [15] Moad G., Solomon D. H., (2005). *The Chemistry of Radical Polymerization* (second edition). ISBN: 978-0-0804-5479-5
- [16] Wittenberg, N.F. (2014). *Kinetics and Modeling of the Radical Polymerization of Acrylic Acid and of Methacrylic Acid in Aqueous Solution*.
- [17] Wittenberg, N.F.G., Preusser, C., Kattner, H., Stach, M., Lacík, I., Hutchinson, R.A. and Buback, M. (2016), Modeling Acrylic Acid Radical Polymerization in Aqueous Solution. *Macromol. React. Eng.*, 10: 95-107. <https://doi.org/10.1002/mren.201500017>
- [18] Lacík, I., Beuermann, S. and Buback, M., (2004), PLP-SEC Study into the Free-Radical Propagation Rate Coefficients of Partially and Fully Ionized Acrylic Acid in Aqueous Solution. *Macromol. Chem. Phys.*, 205: 1080-1087. <https://doi.org/10.1002/macp.200300251>
- [19] Beuermann, S., Buback, M., (2002), Rate coefficients of free-radical polymerization deduced from pulsed laser experiments. *Progress in Polymer Science*, Volume 27, Issue 2, [https://doi.org/10.1016/S0079-6700\(01\)00049-1](https://doi.org/10.1016/S0079-6700(01)00049-1)
- [20] Johannes Barth, Wibke Meiser, and Michael Buback. *Macromolecules* 2012 45 (3), 1339-1345 DOI: 10.1021/ma202322a
- [21] Bally, F., Serra, C., Hessel, V., & Hadziioannou, G. (2011). Micromixer-assisted polymerization processes. *Chemical Engineering Science*, 66(7), 1449–1462. <https://doi.org/10.1016/j.ces.2010.07.026>
- [22] Mosnáček, J., Nicolaÿ, R., Kar, K. et al. Efficient Polymerization Inhibition Systems for Acrylic Acid Distillation: New Liquid-Phase Inhibitors. *Industrial & Engineering Chemistry Research* 2012 51 (10), 3910-3915 DOI: 10.1021/ie201708n
- [23] Meira, G.R., & Oliva, H. (2011). Molecular weight distributions in ideal polymerization reactors: An introductory review. *Latin American Applied Research*, 41, 389-401.
- [24] Takeshi Iwasaki and Jun-ichi Yoshida. *Macromolecules* 2005 38 (4), 1159-1163 DOI: 10.1021/ma048369m